Dear Editor and Referee,

We thank the Referee #2 for the careful and constructive review of our manuscript. The comments and suggestions are of great value to help us to improve the clarity and rigor of the manuscript. We have revised the manuscript and Supplement accordingly. We added 2 new figures in the manuscript, and 21 new figures and 1 table in Supplementary Information.

Especially, we re-did the PMF analysis (compared two factorization methods and three data-treatment approaches), expanded the thermodynamic and kinetic analysis, and revised the descriptions of the particle-size distributions and the 2-D VBS analysis. Kinetic issues are estimated based on Stokes-Einstein equations and validated by Deborah number, while thermodynamics are determined by 2-D-VBS parametrizations and AIOMFAC.

Our point-by-point responses are provided below.

Response to Referee #2

This manuscript investigates the chemical evolution and gas-particle partitioning behavior of cooking-emitted organic aerosols using PAM flow-tube oxidation combined with FIGAERO-CIMS measurements and a 2-D volatility basis set framework. The authors aim to elucidate the compositional evolution and volatility distribution of oxidation products and demonstrate that non-equilibrium partitioning plays a dominant role in cooking-related SOA formation.

The topic is timely and relevant. Cooking emissions have increasingly been recognized as an important urban source of organic aerosols, and their oxidation chemistry and SOA formation mechanisms remain insufficiently understood. The combination of high-resolution FIGAERO-CIMS measurements, PMF-based non-targeted analysis, and volatility characterization provides potentially valuable insights into the evolution of cooking aerosols. The manuscript presents a large dataset and attempts to connect molecular composition with gas-particle partitioning behavior.

Overall, the study has the potential to contribute to the understanding of cooking-derived SOA and its kinetic limitations. However, several aspects of the manuscript require clarification and improvement before it can be considered for publication, as outlined below.

Response: We thank Referee #2 for the careful and constructive assessment. We agree that the previous manuscript overstated diffusion-limited, non-equilibrium partitioning and did not sufficiently describe the methodological assumptions, instrument selectivity, reactor limitations, PMF robustness, and experimental scope. We have therefore expanded the thermodynamic and kinetic analysis, added sensitivity tests, clarified the OFR and iodide-CIMS applicability boundaries, strengthened the PMF validation, stated the partitioning assumptions in the main text, and revised the figures and captions. Detailed responses and the corresponding revised passages and figures are provided below.

A central conclusion of the manuscript is that gas-particle partitioning of cooking-derived SOA deviates significantly from equilibrium due to diffusion limitations. However, the evidence presented for this claim is not entirely convincing. Several alternative explanations should be discussed more thoroughly, including uncertainties in FIGAERO-CIMS quantification, potential thermal decomposition artifacts during desorption, uncertainties in vapor pressure estimation, and limitations associated with the assumption of ideal activity coefficients in the equilibrium calculations. In particular, the comparison of partitioning coefficients relies heavily on estimated vapor pressures and assumed particle composition. Moreover, FIGAERO thermograms are known to produce fragmentation or rearrangement products, which may bias the inferred volatility and therefore affect the interpretation of partitioning behavior.

Response: Thank you for this important comment. We agree that the previous attribution of the observed deviations to particle-phase diffusion was too strong. We expanded Section 3.4 and Section S5 of Supplement S1 to compare gas-phase diffusion, surface desorption, particle-phase diffusion, particle coagulation, oxidation, and Go:PAM residence time. Particle-phase diffusion is the fastest modeled process in both primary and secondary aerosols and is therefore unlikely to be the dominant kinetic resistance. Gas-phase diffusion in the primary-aerosol case has a characteristic time scale of approximately 10^2 s because of the low particle number concentration, whereas gas-phase diffusion in the secondary-aerosol case remains faster than the oxidation and residence time scales. Surface desorption may retain a limited fraction of high-molecular-weight compounds, but its influence on the dominant semi-volatile and intermediate-volatility components is minor.

We also expanded the thermodynamic and measurement-uncertainty analysis. Pure-component vapor pressures were estimated with SIMPOL, activity coefficients with AIOMFAC, and the Kelvin effect with a surface tension of 0.05 N m^{-1}. Liquid-liquid phase separation was evaluated and was not predicted under the modeled conditions. The remaining difference between FIGAERO-derived and theoretical volatilities is discussed in terms of nonexclusive uncertainties, including FIGAERO quantification, filter-mediated evaporation and desorption, thermal decomposition or rearrangement, pure-component vapor-pressure estimates, activity coefficients, and aerosol microstructure. We therefore present the difference as an unresolved measurement-model gap rather than evidence for a single kinetic mechanism.

The revised kinetic and thermodynamic discussion in Section 3.4 reads:

"Gas-particle partitioning is governed by both thermodynamic and kinetic processes. We compared characteristic time scales (τ) for gas-phase diffusion, surface desorption, and particle-phase diffusion with the time scales for particle coagulation, oxidation of cooking precursors (e.g., oleic acid), and residence in the Go:PAM. Detailed equations are provided in Section S5 of Supplement S1, and the results are shown in Figure 4. Particle-phase diffusion is the fastest modelled process in both primary and secondary

aerosols across the investigated OH exposures, with τ values of approximately 10−2–100 s, substantially shorter than the 55 s residence time and the oxidation time scale of primary precursors, implying minor resistance of particle-phase diffusion on gas-particle partitioning under the modelled conditions. Gas-phase diffusion in the primary aerosol is partly limited by the low particle number concentration and has a characteristic time scale of approximately 10^2 s, thus would serve as the main cause of deviation from equilibrium. In the secondary aerosol, gas-phase diffusion remains significant faster than the oxidation and residence time scales resulting in minor kinetic resistance. Surface-desorption time scales increase drastically with molecular weight: species with molecular weight >200 g mol−1 have desorption times longer than the residence time and account for approximately 10% of the total detected mass, whereas species with molecular weight >300 g mol−1 have desorption times longer than 1 h and account for approximately 5%. Surface desorption may therefore retain a limited fraction of high-molecular-weight compounds. C>9O>5 peroxides and auto oxidation products keeping long-chain fatty acid structures (C16,18O>4) would be confined to remain at aerosol phase due to kinetic limits in surface desorption process. Meanwhile, its influence on semi- and intermediate- volatile components remains minor."

"Figure 5 compares estimated and measured volatilities of species in cooking aerosol after accounting for activity coefficients and the Kelvin effect. Liquid-liquid phase separation (LLPS) was also considered and was not predicted under the modeled conditions because none of the species had a particle-phase activity near or above unity (Figure S6.41). Volatility derived from the FIGAERO particle-phase fraction and thermogram peak temperature are generally low and distributed more narrowly than the theoretical estimates. Specifically, based on FIGAERO measurements, the theory overestimates the volatility of the most abundant SVOC to IVOC species by 1-3 order of magnitude, while underestimate the volatility of LVOCs. These gaps are higher for IVOC and LVOC, while closer at the boundary of SVOC to IVOC. Possible explanations on discrepancies between measurement and parametrization include instrumentation limits in FIGAERO measurements, such as hindered evaporation and desorption caused by the FIGAERO filter microstructure (Ylisirniö et al., 2021; Ylisirniö et al., 2025). Another possible cause might be aerosol microstructure influence of functionalized auto-oxidation product or uncertainty on activity coefficients(Wang et al., 2026; Zhang et al., 2024; Chen et al., 2025). Sensitivity test has been done by adding long-chain-fatty-acid related species into measurement result to observe the difference of thermodynamics and kinetics (Figures S6.50-51), showing potential underestimation would not interfere thermodynamic and kinetic estimations, indicating minor effect of fatty-acid-related instrument sensitivity."

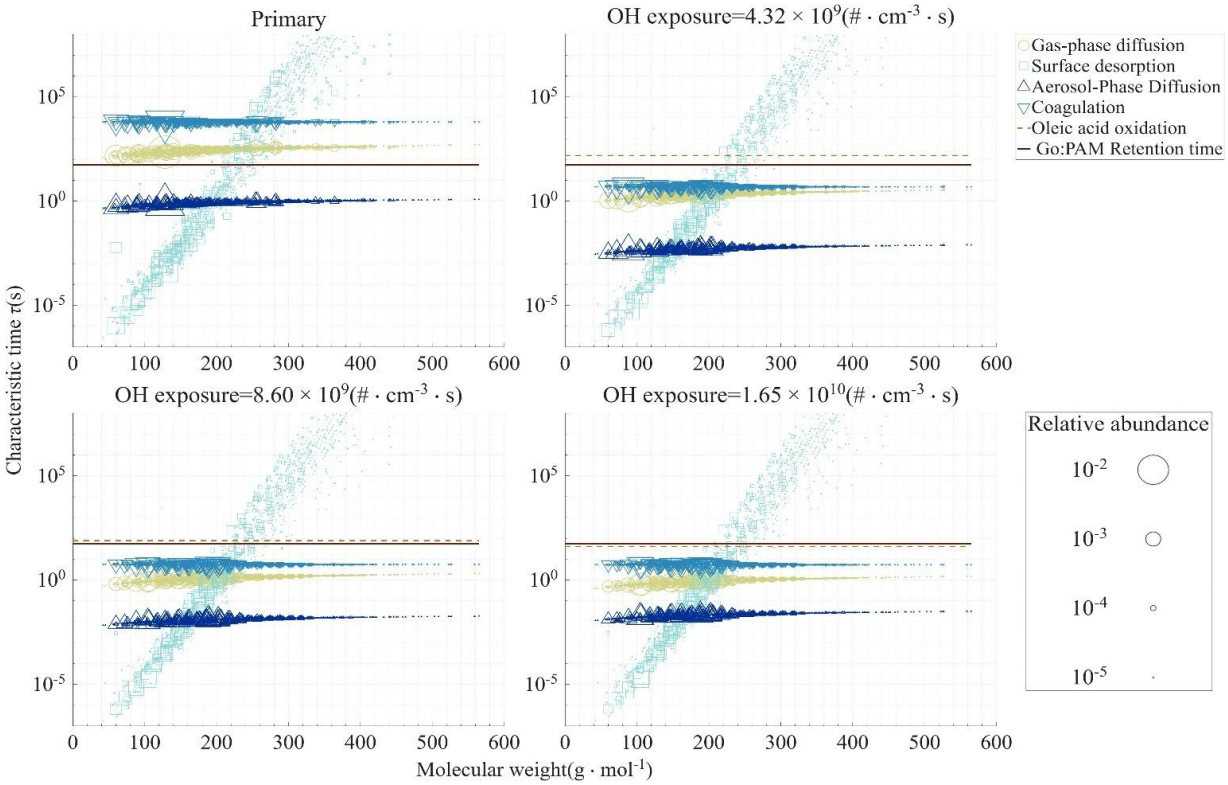

Figure 4:. Characteristic time scales for gas-phase diffusion, surface desorption, particle-phase diffusion, and coagulation across the investigated OH exposures.

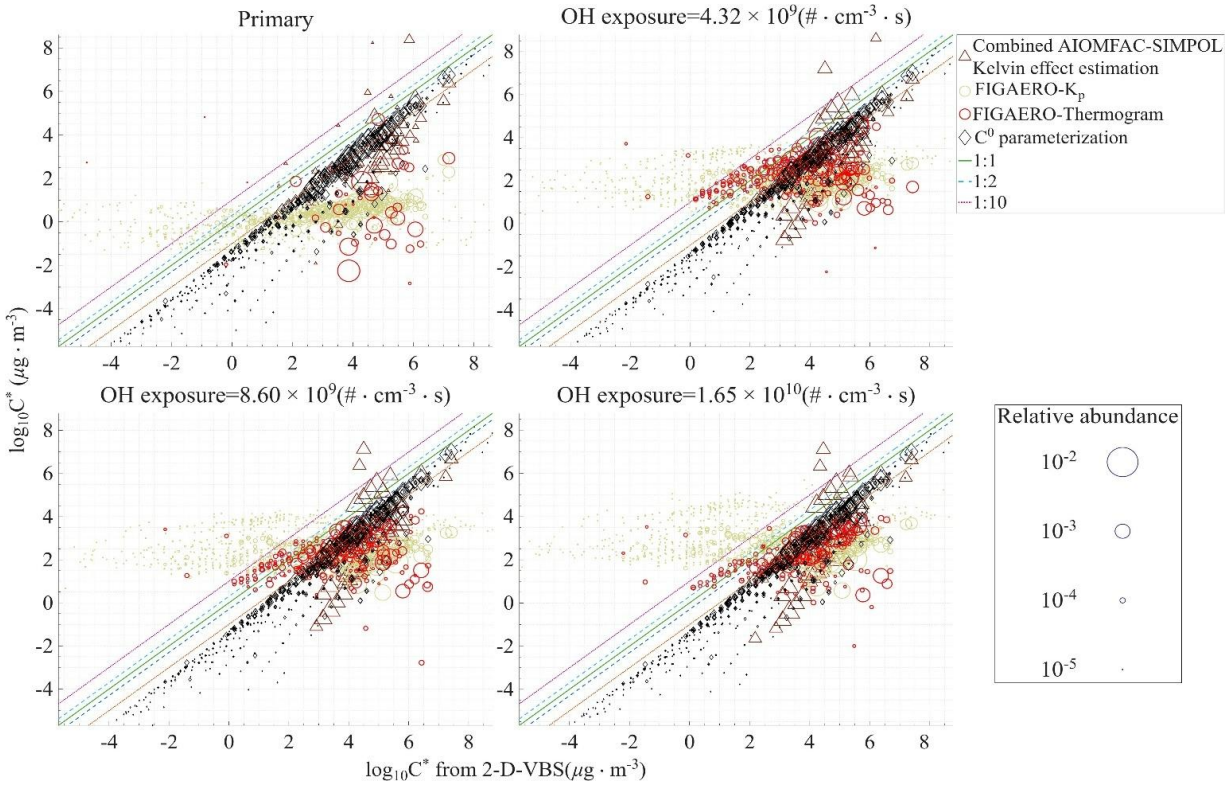

Figure 5:. Comparison of effective saturation concentrations derived from the SIMPOL-AIOMFAC-Kelvin treatment, FIGAERO gas-particle partitioning, FIGAERO thermograms, and the formula-based 2-D VBS parameterization.

The experiments rely on PAM reactor oxidation with OH exposure up to ~1.8×10^{10} cm^{-3} s, corresponding to several hours to days of atmospheric aging. However, PAM reactors can introduce well-known artifacts: unrealistically high oxidant concentrations, secondary photolysis, altered radical chemistry, and enhanced fragmentation. The manuscript should clarify whether artifacts such as OH suppression and RO_2 chemistry differences were considered, and how the chosen oxidation conditions compare to typical indoor or urban atmospheric environments. In addition, cooking emissions are often influenced by NOx chemistry, which is largely absent here due to the use of pure nitrogen carrier gas. The implications of this experimental design for real-world cooking emissions should be discussed more carefully.

Response: Thank you for this important comment. The maximum OH exposure used in this study, approximately 1.8 x 10^{10} molecules cm^{-3} s, corresponds to approximately one day of atmospheric aging if a mean ambient OH concentration of 10^6 molecules cm^{-3} is assumed. We now emphasize that this conversion is only an approximate reference and that an OFR does not reproduce the detailed chemistry of indoor or urban cooking plumes. High instantaneous oxidant concentrations can cause OH suppression, alter RO_2 reaction pathways, promote secondary photolysis, and enhance fragmentation.

The experiment used pure N_2 carrier gas to limit interference from high NO_x with radical oxidation and I-CIMS detection. Consequently, the results should not be directly extrapolated to NO_x-rich cooking plumes. These limitations are now stated in Section 2.1.

The revised experimental-scope and OFR-limitation statement in Section 2.1 reads:

"Briefly, Go:PAM reactor operates under mode OFR254, which OH radical are generated from reaction between O(1D) radicals and water vapor. OFR254 represent atmospheric oxidation processes dominated by OH radical at low-medium NOx concentration(Peng and Jimenez, 2020). OH exposure in the Go:PAM system is controlled by varying ozone concentration, relative humidity, and the experimental sample gas flow rate through the Go:PAM reactor. OH exposure is estimated using semi-empirical parametrizations in OFR254 recommended by Peng et al., based on measured OH reactivity, ozone concentration and relative humidity (Peng et al., 2016). Cooking experiments were conducted in a custom-made fry pan directly connect to pure nitrogen as carrier gas to avoid interference of high NOx in ambient air on radical oxidation and I-CIMS detection. Cooking emissions are generated by heating corn oil to 120~130 °C, representing the evolution of widely used cooking oil during typical domestic cooking activities, and to certain extent representing frying and stir-frying activities widely used in both Eastern and Western cooking types(Rogge et al., 1991; He et al., 2004; Abdullahi et al., 2013; Bandowe et al., 2021).For reproducibility, we performed 4 times. It should be noted that this experiment represents a controlled, low-NOx oil-heating case rather than the full range of cooking emissions, thus the results should not be directly

extrapolated to NOx-rich cooking plumes. The use of an OFR can introduce OH suppression, altered RO2 chemistry, secondary photolysis, and enhanced fragmentation; therefore, the OH-exposure-to-atmospheric-age conversion is used only as an approximate reference. Detailed experimental conditions and setup are presented in Section S1, Supplement Information 1."

The authors note that iodide-CIMS detection may underestimate low-oxygenated or nonpolar species, such as long-chain hydrocarbons and fatty acids. This limitation could strongly influence the conclusions. For example, the reported small molecular size of primary aerosols and the inferred dominance of S/IVOCs may partly reflect instrumental detection bias. The manuscript should clearly discuss the detection efficiency of iodide-CIMS for cooking emissions, potential missing compound classes, and the implications for interpreting 2-D VBS distributions.

Response: We agree that iodide-CIMS selectivity must be stated explicitly. Iodide adduct ionization is generally more sensitive to polar and oxygenated compounds and can underrepresent weakly oxygenated or nonpolar species, including portions of the long-chain hydrocarbon and fatty-acid emissions. The reported molecular-size, oxidation-state, and 2-D VBS distributions therefore describe the detectable iodide-CIMS ion ensemble rather than a mass-complete representation of cooking emissions. This limitation is most important for the primary aerosol and constrains quantitative claims about the dominance of S/IVOCs across all emitted material.

To test whether possible underestimation of long-chain-fatty-acid-related species would alter the conclusions, we added oleic acid and selected C_{18} oxidation products at a prescribed signal contribution corresponding to 10% of the total ion intensity. The sensitivity analysis produced only minor changes in the modeled thermodynamic and kinetic patterns (Figures S6.50-S6.51). We therefore retain the instrument-selectivity limitation while concluding that this perturbation does not materially change the principal partitioning interpretation.

The revised applicability statement and sensitivity-test description in Section 2.2 and Section S5 of Supplement S1 read:

"Iodide-CIMS is selective toward polar and oxygenated compounds and may underrepresent weakly oxygenated or nonpolar material. Accordingly, the molecular-composition and 2-D VBS distributions reported here describe the detectable iodide-CIMS ion ensemble rather than a mass-complete representation of all cooking emissions (Iyer et al., 2016)."

"To account for potential effect on underestimation on long-chain-fatty acid related species, we performed a sensitivity test by adding oleic acid and $C_{18}H_{32}O_{4\text{-}8}$ oxidation product to the measured composition. The concentration is set as corresponding to 1/10

of the total ion intensity. The comparison between thermodynamics and kinetics are shown in Figures S6.50-51."

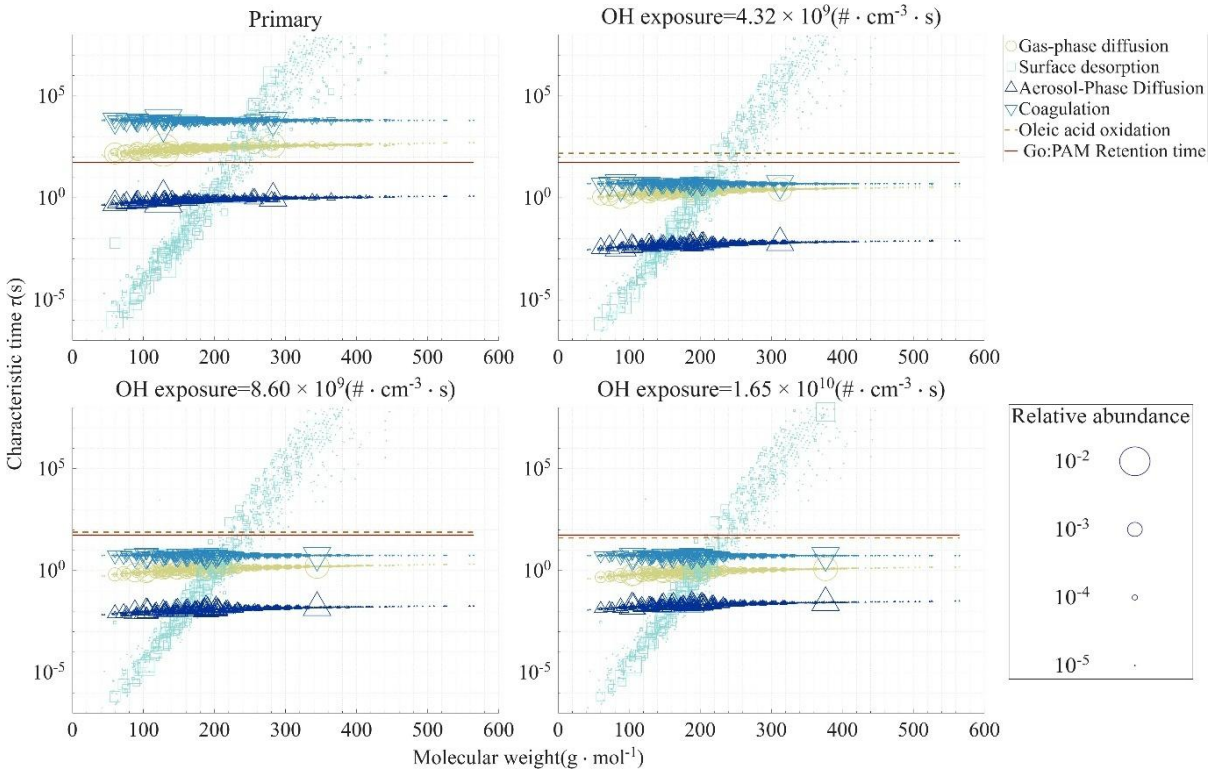

Figure S6.50: Sensitivity analysis of the influence of potentially underestimated long-chain-fatty-acid-related species on the modeled kinetic time scales.

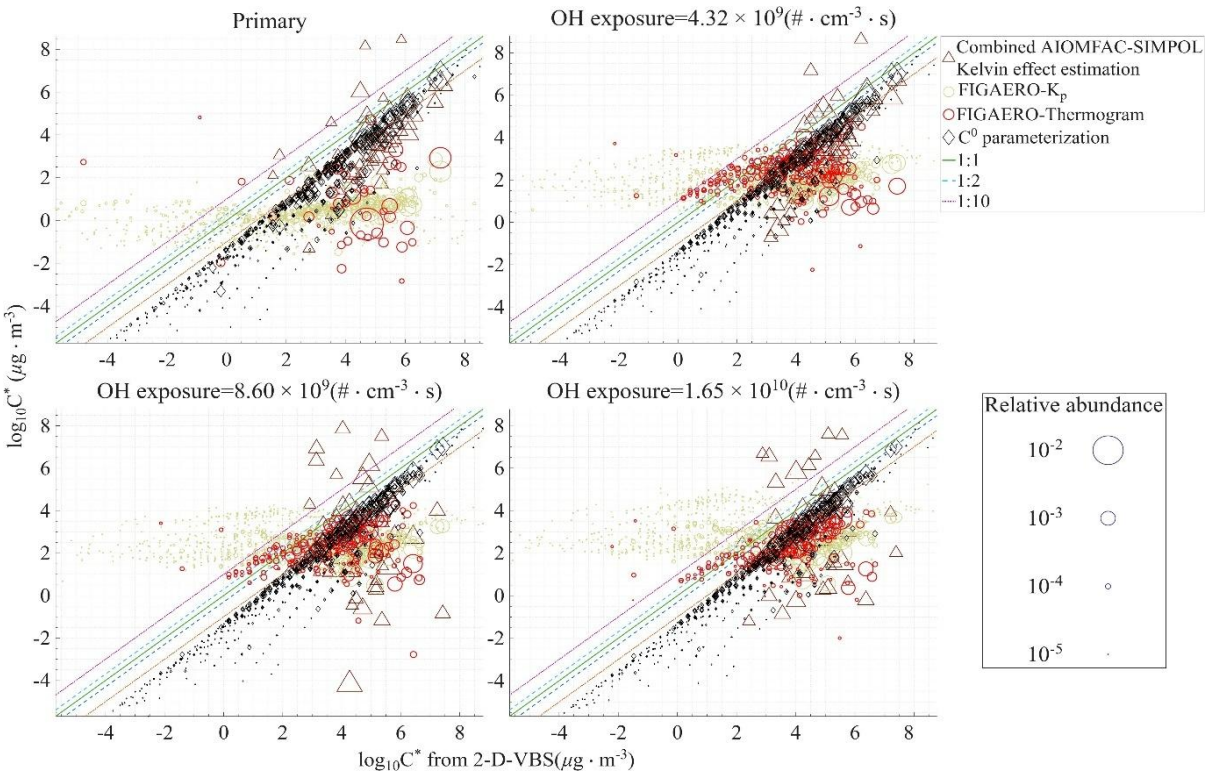

Figure S6.51:. Sensitivity analysis of the influence of potentially underestimated long-chain-fatty-acid-related species on the thermodynamic comparison.

The PMF analysis identifies 13 factors representing volatile, semi-volatile, and low-volatility species. However, the physical interpretation of these factors appears somewhat speculative. For example, the assignment of factors to specific oxidation generations, the identification of fatty-acid cleavage products, and the interpretation of thermogram-derived volatility should be supported by stronger evidence. The authors should clarify how the optimal number of factors was determined, assess the robustness of the results with respect to changes in PMF configuration, and discuss whether the identified factors are chemically meaningful beyond statistical separation.

Response: Thank you for this suggestion. We expanded Section S4 to compare two factorization methods, ME-2 PMF and MATLAB NNMF, using three data treatments: the joint gas- and particle-phase time series, the particle-phase-only dataset, and a normalized trend-only dataset. Solutions were evaluated using Q/Q_{exp}, RMSE, explained absolute variance (RatioVar), time-resolved absolute relative residuals, and unexplained variation. Factor-number turning points were assessed together with local residuals and the physical interpretability of the thermograms. Pairwise spectral contrast angles are reported in Figure S4.13.

ME-2 PMF with the full time-series dataset was retained because it explicitly accounts for measurement uncertainty and performed better when the uncertainty-weighted and local residual metrics were considered. The 13-factor solution was selected because adding factors did not materially improve the global or local diagnostics and reduced physical interpretability.

We also reorganized the factor interpretation using volatility classes (V, SV, and LV), compositional features, and the OH-exposure stage at which each factor is most abundant. Molecular structures are described as possible or putative assignments rather than unique identifications.

The revised PMF-validation and factor-interpretation text in Section S4 and Section 3.3 reads:

> *"Figures S4.1-S4.3 show changes of the global goodness parameters of ME-2 PMF and MATLAB® NNMF with adding factors. MATLAB® NNMF exhibits better goodness performance on global goodness parameters without considering measurement uncertainty such as lower RMSE and higher RatioVar, especially at factor numbers below 10, while ME-2 PMF shows significant better performance considering measurement uncertainty using Q/Qexp. Figures S4.4-S4.6 depicted time series of local goodness parameters such as absolute relative residual. We concluded from Figs. S4.4-4.6, that ME-2 PMF shows better performance than MATLAB® NNMF, considering interpreting evolution of composition in oxidation of cooking emission. Only when data pre-treat method are trend analysis methods that normalize speculated time series of detected ions to maximum value, ME-2 PMF and MATLAB® NNMF have comparable performance. Among data pre-treat processes, while utilizing ME-2 PMF as the factorization algorithm, as Figures S4.10-S4.12 show, full time-series data shows slightly better performance than particle-phase only data and obvious advantage over time series normalized to maximum point of each detected compound. On the contrary, MATLAB® NNMF method favors data process adopting normalized full time series than particle-phase only and full time series, especially at duration corresponding to measurement of primary cooking emissions, shown in Figures S4.7-S4.9. In conclusion, we would prefer choosing ME-2 PMF as factorization algorithm, select full time series data as main data pre-treat method for PMF in this article, while treat results of particle-phase only data to volatility and partitioning results as reference. Based on chosen ME-2 PMF methods and basic data pre-treat methods, we would select the result with 13 factors as the most interpretable PMF results. The reason is, adding factor into PMF will not lead to significant improvements on global goodness and local goodness on both time series and compound axes, shown in Figure S4.1, S4.12 and Table S4.1."*

> *"The FIGAERO-CIMS results are divided into 13 factors, including 5 pure gas-phase factors, 3 semi-volatile factors with considerable and comparable amounts both in gas phase and aerosol phase, and 4 pure aerosol-phase factors. Factors are listed in Fig. 3 and classified by its volatility (partitioning coefficient Kp while total amount is countable) and oxidative state (mean oxidative state OSC and evolution with enhancement of OH exposure). Detailed factor classification and interpretation procedure is shown in Section S4 of the Supplement S1."*

"12 interpretable factors are classified as 3 categories, considering its volatility represented by peak temperatures of factor thermograms and FIGAERO-CIMS measured gas-particle partitioning coefficient Kp, shown in Figure S4.14. Factors mainly or even almost present in gas phase are named volatile factors "V-x". Factors abundant in both gas phase and aerosol phase factors are called semi-volatile factors "SV-x". Mostly particle phase factors are classified low-volatile factors "LV-x". Factors among each volatility categories are further distinguished and named by oxidative state, molecular composition and possible origin."

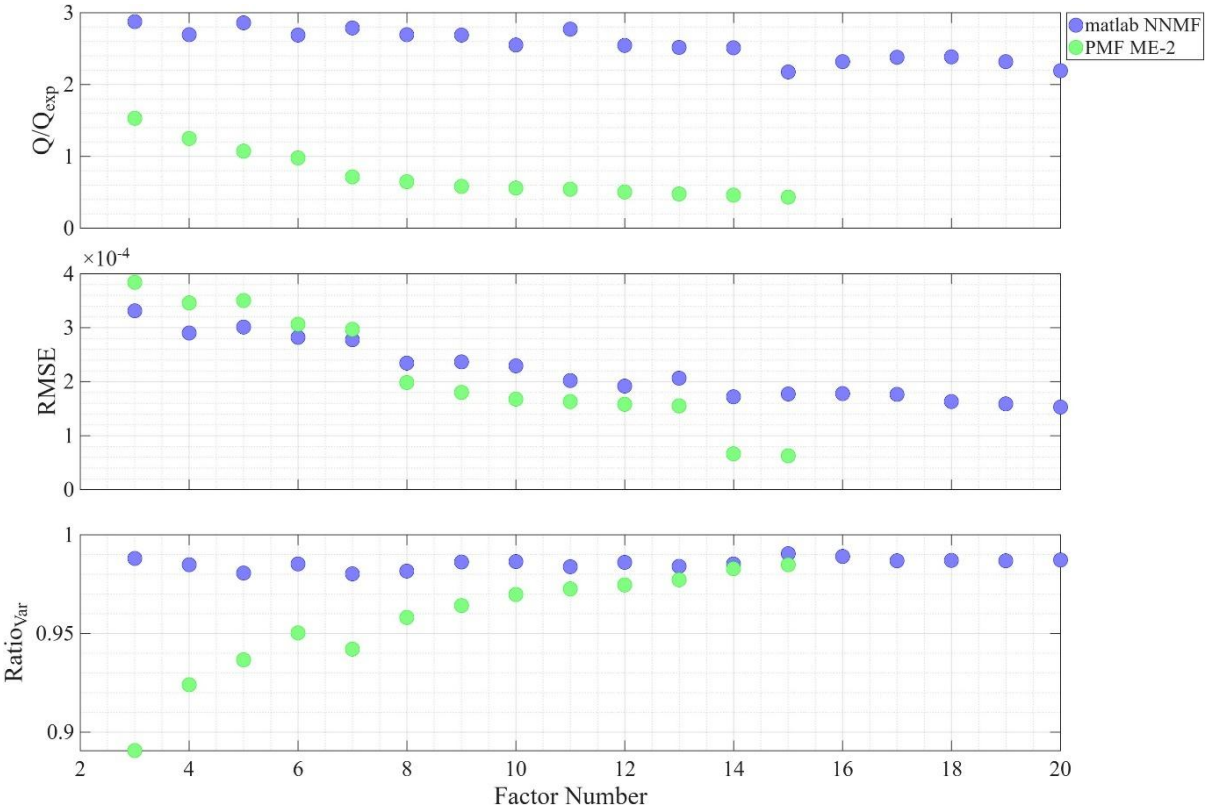

Figure S4.1:. Evolution of Q/Qexp, RMSE, and RatioVar with factor number for ME-2 PMF and MATLAB NNMF using the full FIGAERO-CIMS time series.

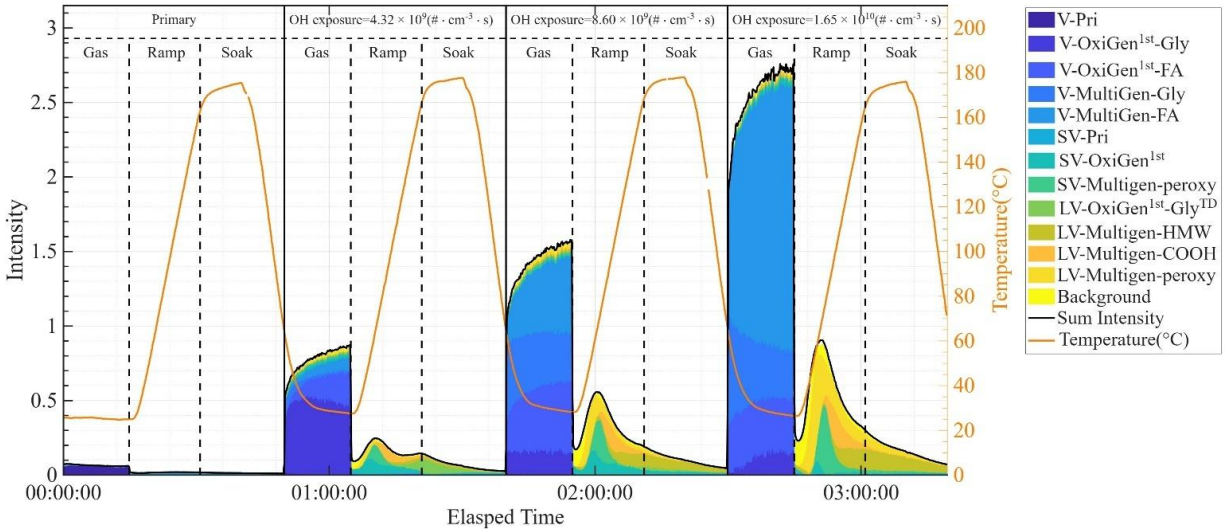

Figure 3: Time series of the classified 13-factor ME-2 PMF solution across the primary and oxidized conditions.

The partitioning analysis presented in Figure 4 compares experimental Kp values with equilibrium predictions. However, the methodology used to derive Kp from the FIGAERO data is complex, and the assumptions underlying the equilibrium calculations are not clearly described in the main text. Key parameters, such as the particle-phase molecular weight, organic mass concentration, and activity coefficients, should be explicitly stated. At present, much of the derivation is only described in the Supplement, which reduces clarity and makes it difficult for readers to fully assess the analysis.

Response: Thank you for this suggestion. We expanded Section 2.5 and Section 3.4 to state the quantities and assumptions used in the partitioning calculation. Experimental K_p is derived from paired FIGAERO gas- and particle-phase measurements together with the measured organic-aerosol mass concentration; the OA mass concentrations are reported in Table S6.1. For the equilibrium calculation, pure-component vapor pressure is estimated with SIMPOL, activity coefficients are calculated with AIOMFAC, the organic mass fraction is taken as unity, the mean particle-phase molecular weight is calculated as a concentration-weighted value for the detected composition, and the Kelvin effect is included as described in Section 2.5 and Section S5. The complete derivation remains in Section S5 of Supplement S1.

The revised figure organization separates the kinetic and thermodynamic comparisons: Figure 4 presents the characteristic kinetic time scales, whereas Figure 5 compares the FIGAERO-derived and theoretically estimated effective saturation concentrations.

The revised methodological description in Section 2.5 reads:

"Experimental Kp values are derived from paired FIGAERO gas- and particle-phase measurements together with the measured organic-aerosol mass concentration reported in Table S6.1. For the equilibrium calculation, the organic mass fraction is assumed to be

unity, the mean particle-phase molecular weight is calculated as an concentration-weighted value for the detected organic composition."

"For fingerprint species extracted from CIMS detection based on PMF and ordinal analysis(Buchholz et al., 2020a; Kong et al., 2021), saturation vapor pressure are estimated utilizing SIMPOL(Pankow and Asher, 2008), and activity coefficients are calculated by AIOMFAC, and to ensure whether liquid-liquid phase separation will occur within cooking POA and SOA, , aerosol phase molar-fraction based activity are calculated (Zuend and Seinfeld, 2012) (https://aiomfac.lab.mcgill.ca/)."

Trace amounts of sulfur appear in the reported elemental compositions, but the manuscript does not discuss their origin. Since sulfur-containing compounds in cooking emissions are often associated with ingredients such as garlic or onions, clarification is needed. However, the experiments appear to involve heating corn oil only, without food ingredients. The authors should therefore explain whether the detected sulfur species originate from cooking emissions, background contamination, or uncertainties in molecular formula assignment.

Response: The experiment used corn oil only and did not include garlic, onion, or other food ingredients. We therefore do not attribute the trace sulfur-containing formulas to ingredient-derived cooking emissions. Given their low abundance, these signals may reflect instrument or laboratory background, trace contamination, or uncertainty in molecular-formula assignment. We now state this uncertainty explicitly and exclude the trace sulfur-containing formulas from mechanistic source interpretation.

The corresponding applicability statement in Section 2.2 reads:

"Trace sulfur-containing formulas were not used for mechanistic source interpretation because the corn-oil-only experiment contained no sulfur-rich food ingredients and the low-abundance signals may reflect background, contamination, or formula-assignment uncertainty(Zhang et al., 2020; Song et al., 2022)."

Several details should be clarified: the exact composition of the cooking emissions (oil only vs food ingredients), repeatability of the experiments, and the number of experimental replicates. Currently, only corn oil heating at 120-130 °C is described. This may not represent typical cooking conditions.

Response: The present study is a controlled oil-heating experiment using corn oil at 120-130 degrees C. It is intended to isolate emissions originating from heated cooking oil and does not represent the full diversity of cooking styles, ingredients, or temperatures. Four experimental runs were conducted. The experimental scope, replicate number, and applicability boundary are stated in Section 2.1.

The revised experimental-scope statement in Section 2.1 reads:

"Cooking emissions are generated by heating corn oil to 120~130 °C, representing the evolution of widely used cooking oil during typical domestic cooking activities, and to certain extent representing frying and stir-frying activities widely used in both Eastern and Western cooking types(Rogge et al., 1991; He et al., 2004; Abdullahi et al., 2013; Bandowe et al., 2021).For reproducibility, we performed 4 times. It should be noted that this experiment represents a controlled, low-NOx oil-heating case rather than the full range of cooking emissions, thus the results should not be directly extrapolated to NOx-rich cooking plumes."

Figures: The font size in several figures is too small and should be enlarged for readability (e.g., Figure 1(e)). In addition, the subpanel label "(e)" is not clearly marked in the figure and should be added to match the caption.

Response: Thank you for pointing this out. We revised Figure 1 to improve the readability of the panel labels and ensured that panel (e) is clearly marked and described consistently in the caption. We also checked the labels, captions, and cross-references for the remaining main-text and supplementary figures. No plotted data were changed.

The revised Figure 1 caption reads:

"Figure 1 Primary and Secondary aerosol size & mass distribution evolution with OH exposure increases. (a) (b)illustrate size and mass distribution of primary particles, (c) (d) size and mass distribution of secondary aerosols at OH exposure 0.1~1.8×1010 cm-3 s. (e) exhibits mass concentration evolution with oxidation process from primary to OH exposure 1.8×1010 cm-3 s."

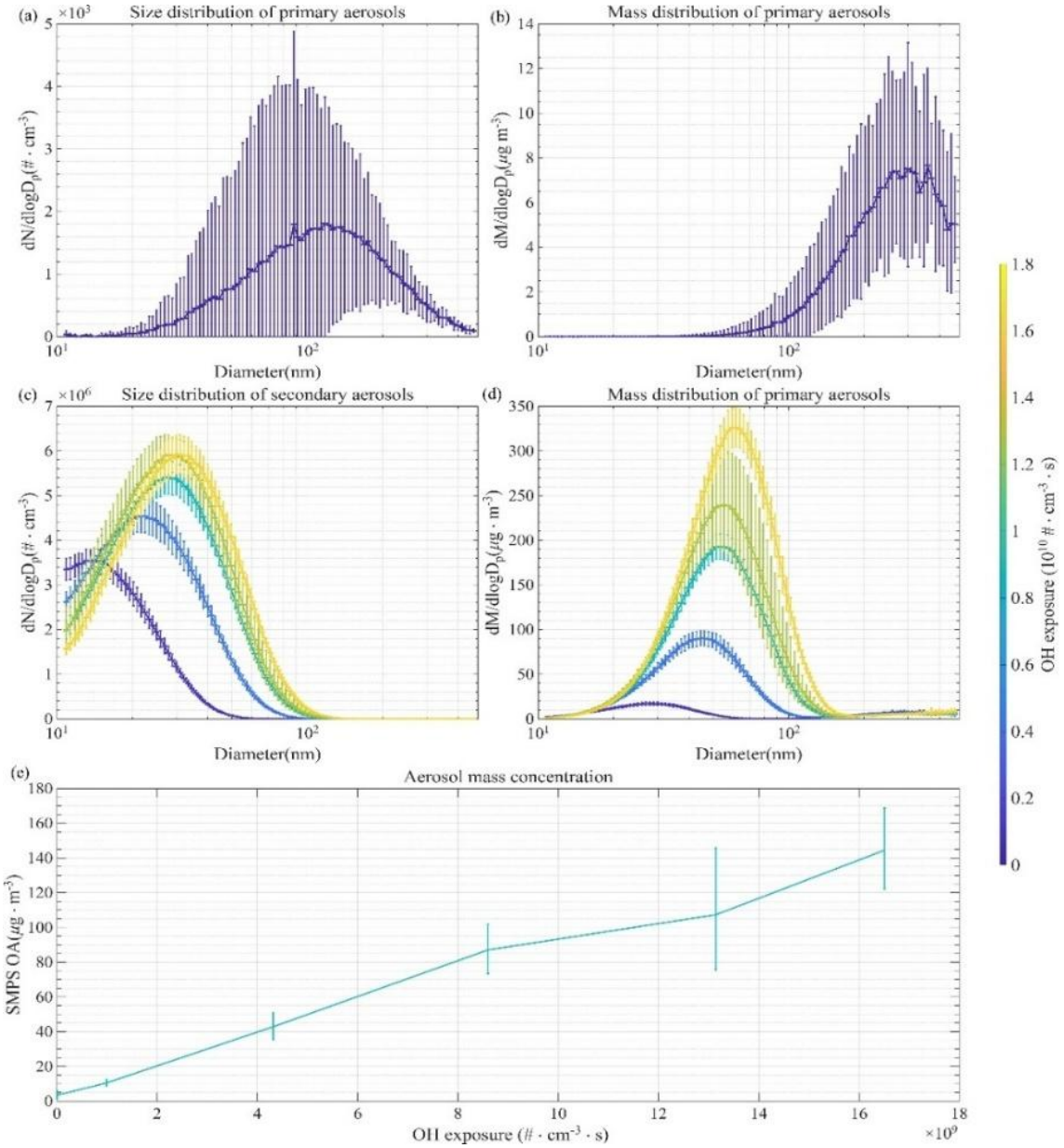

Figure 1: Primary and Secondary aerosol size & mass distribution evolution with OH exposure increases. (a) (b)illustrate size and mass distribution of primary particles, (c) (d) size and mass distribution of secondary aerosols at OH exposure 0.1~1.8×10^{10} cm^{-3} s. (e) exhibits mass concentration evolution with oxidation process from primary to OH exposure 1.8×10^{10} cm^{-3} s. panel (e) are clearly marked.